Experimental Verification of an Optical Vortex Coronagraph

Jae Hoon Lee,[1] Gregory Foo,[1] Eric G. Johnson,[2] and Grover A. Swartzlander, Jr.[1,*]

[1]College of Optical Sciences, University of Arizona, Tucson, Arizona 85721, USA
[2]College of Optics and Photonics, University of Central Florida, Orlando, Florida 32816, USA

(Received 14 April 2006; published 2 August 2006)

A coronagraph designed for high contrast imaging applications has been experimentally tested using coherent laser light and a vortex mask of topological charge $m = 2$. Intensity contrast values of 95% were achieved in this first verification of the scheme. Improvements for approaching the theoretical value of 100% are suggested.

DOI: 10.1103/PhysRevLett.97.053901 PACS numbers: 42.30.Kq, 42.25.Fx, 97.82.Cp

Optical vortices occur as natural modes in both highly symmetric systems, such as lasers and optical fibers, and in asymmetric systems that create caustics or speckle [1]. Such beams have been termed "twisted light" owing to the helicoidal wave front and "phase singularities" owing to the undefined phase at the vortex core. Recent interest in optical vortices has developed owing to beam-shaping techniques such as computer generated holography and diffractive optics. Optical scientists are finding increasing use for these once esoteric beams, e.g., optical tweezers [2], high-resolution fluorescence microscopy [3], lithography [4,5], quantum entanglement [6–8], and extrasolar planet detection [9,10]. Advanced fabrication techniques [11,12] and achromatic designs [13] may soon allow the formation of nearly ideal vortex beams across a broad band of visible wavelengths. Subwavelength grating structures may be used to achieve these goals in the infrared [10,14].

An optical vortex coronagraph was recently proposed for the detection of extrasolar planets whereby the traditional occulting disk was replaced by a spiral phase mask [9]. This approach promises superior performance compared to the standard Lyot coronagraph and other modern variants [15,16]. Here we demonstrate the formation of a high contrast blind spot that extinguishes the image of a bright point source without attenuating light from an adjacent source. Means of approaching a contrast of 100% are suggested.

The vortex coronagraph, depicted in Fig. 1, has a vortex phase mask in the back focal plane of an objective lens L_2. The circular entrance pupil is uniformly illuminated with a collimated plane wave, as may occur for starlight reaching a space-based telescope. When the source lies on the optical axis, the field at the input face of the phase mask produces a diffraction-limited Airy disk intensity pattern. This field E_{in} is proportional to $J_1(u)/u$, where $u = k\rho R_2/f_2$, J_1 is the Bessel function of the first kind of order one, k is the wave number, ρ is the transverse radial coordinate, and R_2 and f_2 are the radial size and focal length of the lens L_2, respectively. In the laboratory, this is achieved by use of lens L_1 and a quasipoint source. For an afocal Keplerian telescope, the beam in the back focal plane of lens L_3 is related to a Fourier transform of the function $E_{\text{out}} = tE_{\text{in}}$, where t is the field transmission function of the phase mask. When the vortex mask is absent, an image of the pupil at lens L_2 appears in this exit pupil plane.

The field transmission function of the vortex mask may be written $t = \exp(im\theta)$, where m is called the topological charge and the azimuth θ is measured about the vortex axis in the transverse plane. The vortex axis is made to coincide with the optical axis of the system. As the beam propagates, it develops a dark core [17,18], as depicted in Fig. 2(a). The phase (modulus 2π) of the beam is represented in Fig. 2(b) for the case $m = 2$.

The vortex coronagraph takes advantage of a striking diffraction pattern that occurs in the optical system [see Fig. 2(c)]. Rather than forming a uniformly illuminated disk, the entire beam is diffracted outside the disk. This diffraction phenomenon occurs only for an on-axis point source at infinity. The intensity in the pupil region vanishes when $|m| = 2$ [9] or any other even integer [10]. This is remarkable because a vortex beam typically exhibits a single point of zero intensity [see Fig. 2(a)]. The disk area is equal to $\pi R_2'^2$, where $R_2' = R_2 f_3/f_2$ is the magnified radius of the entrance pupil. Outside the disk, the intensity decreases monotonically as $(R_2'/\rho)^4$ for the case $|m| = 2$. To function as a coronagraph, a diaphragm or

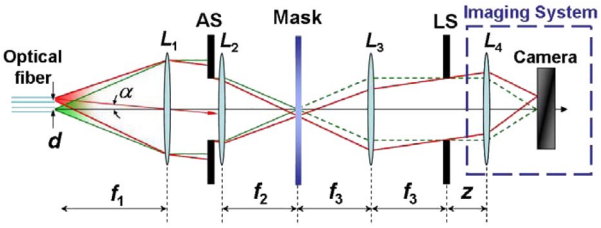

FIG. 1 (color online). Schematic diagram of a collimator and optical vortex coronagraph. Optical fibers serve as quasipoint sources of red and green light. The collimating lens L_1 has a focal length $f_1 = 1$ m and radius $R_1 = 50$ mm. The aperture stop (AS) is of radius $R_2 = 6$ mm. Lenses L_2 and L_3 have respective focal lengths $f_2 = 0.3$ m and $f_3 = 0.25$ m, with a vortex mask in the afocal plane of the telescope. The Lyot stop (LS) is of radius R_{Lyot}. Imaging system: Lens L_4 with focal length $f_4 = 0.085$ m or 0.1 m.

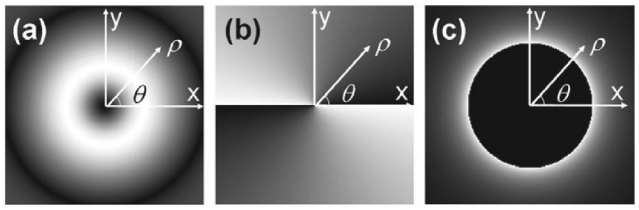

FIG. 2. Calculations for an $m = 2$ vortex. (a) Typical amplitude profile with zero intensity point. (b) Phase profile with relative phase 0 (2π) shown as black (white). (c) Amplitude at the coronagraph exit pupil for an on-axis light source.

"Lyot stop" of radius $R_{\mathrm{Lyot}} \leq R_2'$ is inserted to prevent the diffracted light from reaching the imaging system.

In contrast, incoming light having a wave vector subtending the optical axis at an angle exceeding the resolution angle $0.61\lambda/R_2$ propagates through the Lyot stop and is recorded by the imaging system. Such a wave does not focus on the vortex axis but rather at a region where the mask resembles a wedge. There the beam is simply deflected by an angle of less than $mR_2/1.22\pi f_2$. An observer looking through the system therefore finds a blind spot along the optical axis and an otherwise mostly normal image.

For experimental convenience, point sources at two easily distinguishable wavelengths were produced by coupling green ($\lambda_{\mathrm{green}} = 532$ nm) and red ($\lambda_{\mathrm{red}} = 633$ nm) laser beams into separate multimode optical fibers of 125 μm cladding diameter. The light was collimated by placing lens L_1 a distance of f_1 from the fiber ends. The aperture stop (AS) was uniformly illuminated with light from both fibers. A Lyot stop was inserted in the back focal plane of L_3. An imaging system comprising a lens and a detector array (Canon EOS 10D) was used to record images. Images of the fiber sources were produced with an 85 mm zoom camera lens. The exit pupil was recorded using a single biconvex lens of focal length $f_4 = 100$ mm.

Our 4 mm $\times$ 4 mm fused silica vortex phase mask was designed to produce a topological charge of value $m = 2$ at λ_{green}. The fabricated surface, depicted in false color in Fig. 3, varied stepwise over 16 steps. The pitch measured 2.2 ± 0.1 μm on a Veeco interferometric profilometer. The transmission of light into the odd and zero orders of topological charge owing to the stepped surface are calculated to be negligible, assuming no mask fabrication errors. Additive lithographic techniques were used to first expose a photoresist layer on fused silica with the aid of four binary master masks and then mill the fused silica with reactive ion etching [11].

As expected, the vortex mask produced striking results. The pupil image in Fig. 4(a) confirms that the green beam is diffracted outside the area of the exit pupil, while the red beam uniformly fills the exit pupil. The focal spot of the green beam was centered on the vortex axis, whereas the red beam was roughly 150 μm from this point. The angular distance between the two light sources was $\alpha = \arctan(d/f_1) \approx 0.50$ mrad, which is equivalent to 9.3 times the diffraction limited angular resolution $\alpha_{\mathrm{diff}} = 0.61\lambda/R_2 \approx 0.054$ mrad. The radius of the entrance and exit pupils were $R_2 = 6$ mm and $R_2' = (f_3/f_2)R_2 = 5$ mm, respectively. Evidence of the stepped phase mask is seen as diffraction streaks tangential to the disk in Fig. 4(a).

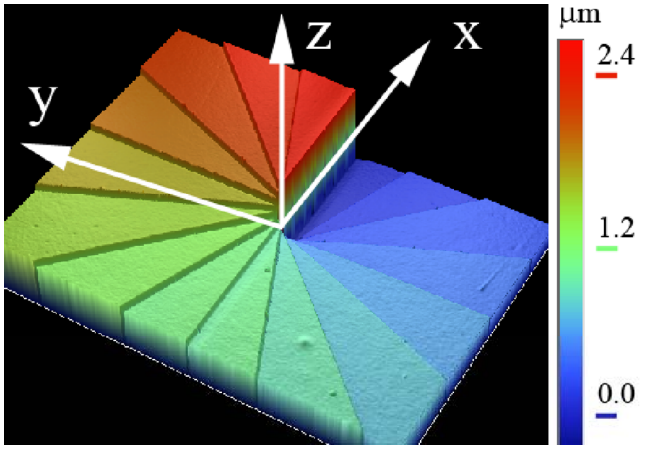

FIG. 3 (color online). False color surface profile of 16-step vortex mask.

Images of the fiber ends are shown in Fig. 4(b) for the case where the Lyot stop was made slightly smaller than

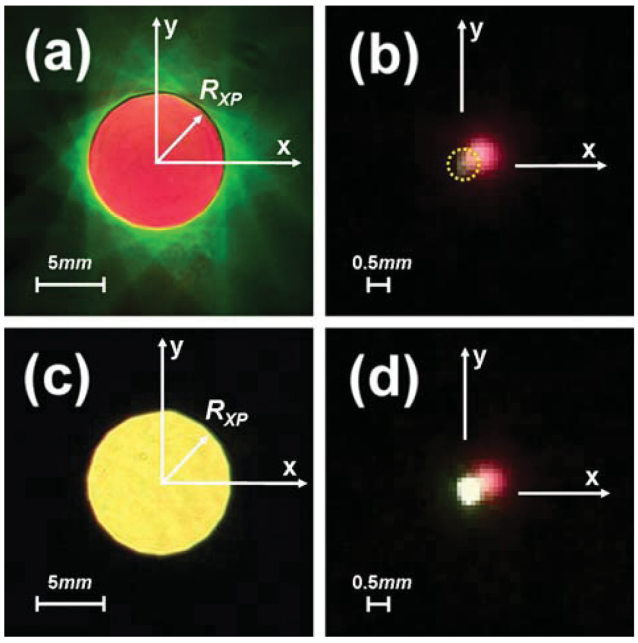

FIG. 4 (color). True color images for green (red) on-axis (off-axis) sources. Top row: Images with vortex mask in place. (a) Exit pupil. (b) Optical fibers. A dotted circle indicates the missing green beam. Bottom row: Images without the vortex mask. (c) Exit pupil (superimposed red and green beams cast a yellow hue). (d) Optical fibers.

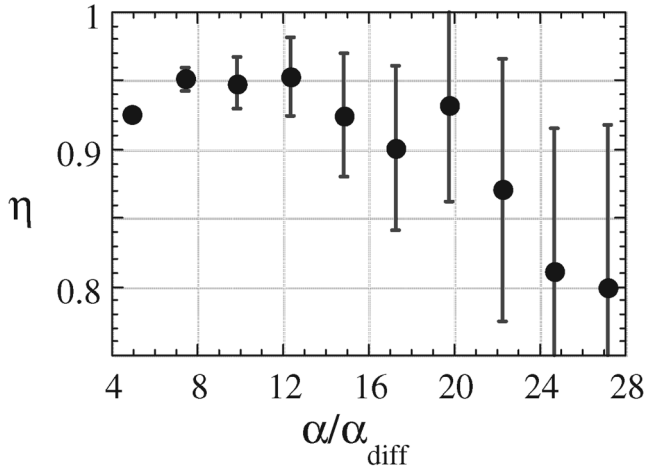

FIG. 5. The intensity contrast for the green beam as a function of angular distance. The contrast is roughly 95% from $7.4\alpha_{\text{diff}}$ to at least $12.4\alpha_{\text{diff}}$.

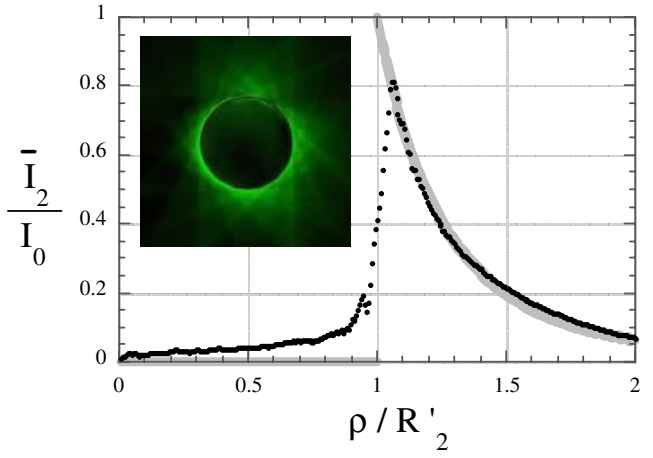

FIG. 6 (color online). Average radial intensity profile of the on-axis beam at the exit pupil plane for experimental (data points) and theoretical (gray line) cases. The inset shows the true color image of the exit pupil.

the exit pupil ($R_{\text{Lyot}} \approx R_2'$). Although the red source is clearly evident in Fig. 4(b), the green source is barely visible, as expected. For comparison, we removed the vortex mask and recorded images shown in Figs. 4(c) and 4(d). In this case, both beams fill the exit pupil, producing a yellow hue, and the imaged green point source saturates the camera. Comparing the red beams in Figs. 4(b) and 4(d), we see the red beam remains qualitatively unchanged when the vortex mask is removed.

With the red beam turned off and with $R_{\text{Lyot}} = 0.7R_2'$, we recorded images of the green light source with and without the vortex mask in place, i.e., $m = 2$ and 0, respectively. The intensity contrast $\eta(\rho) = (\bar{I}_0(\rho) - \bar{I}_2(\rho))/(\bar{I}_0(\rho) + \bar{I}_2(\rho))$ calculated from these measurements is plotted in Fig. 5, where $\bar{I}_m(\rho) = \oint I_m(\rho, \theta)d\theta/2\pi$ is the mean intensity along a circle of radius ρ. The contrast is roughly 95% for angular distances ranging from $7.4\alpha_{\text{diff}}$ to at least $12.4\alpha_{\text{diff}}$. At larger angular distances, the signal to noise ratio was too poor to determine reliable values of contrast. High contrast values at smaller angular distances were confounded by aberrations.

The theoretically expected contrast of 100% was not achieved owing to the leakage of green light through the Lyot stop, as evident in the inset image in Fig. 6. The systematic errors included (1) aberrations, (2) multiple reflections, and (3) mask fabrication errors. The first two may be corrected by use of better quality optics, single mode optical fiber sources, and antireflection coatings. Palacios has recently determined that aberration errors may be minimized by use of larger values of m [16]. Correcting the third error requires subwavelength control of the lithographic process, e.g., uniform etching rates. To quantify the leakage problem, we calculated the normalized mean radial intensity profile $\bar{I}_2(\rho)/I_0$, where $I_0 = \int_0^\infty \int_0^{2\pi} \rho I(\rho, \theta)d\theta d\rho/\pi R_2'^2$. Outside the dark hole, the intensity decreased, according to a power-law fit, as $\bar{I}_2(\rho)/I_0 = (\rho/R_2')^\gamma$, where $\gamma = -3.96 \pm 0.02$. This exponent agrees well with the expected value of $\gamma = -4.0$. Inside the dark hole, the intensity may be expressed as $\bar{I}_2(\rho)/I_0 = C_0 + C_2(\rho/R_2')^4$, where $C_0 = 0.028 \pm 0.001$ and $C_2 = 0.142 \pm 0.004$. The constant offset intensity C_0 is attributed to the nonvortex mode of the transmitted beam owing to mask fabrication errors. The value of C_0 may be related to the mask surface error from the approximation $C_0 = (\pi\delta m)^2/3$, assuming $\delta m \ll 1$ is the topological charge error in the vicinity of the vortex axis [19]. Thus, we estimate $\delta m \approx 0.092$, which represents an error of 4.6% of the desired value of m. This error matches the measured surface error of our vortex mask. The quartic term may be attributed to aberrations and ghost images and suggests the need for well-corrected optics having antireflection coatings.

In conclusion, an optical vortex coronagraph was experimentally tested using a 16-step vortex phase mask having a topological charge of $m = 2$. The theoretical prediction of the formation of a black disk spanning the exit pupil has been verified. Analysis of the data has helped identify the experimental errors that limited the measured contrast to 95%. A contrast approaching 100%, as required for the detection of extrasolar planets, may be achieved by use of diffraction limited optical components having antireflection coatings and a high quality vortex mask.

We thank David M. Palacios (Jet Propulsion Laboratory, Pasadena, California) for discussions about contrast measurements, Joanna Schmit (Veeco Inc., Metrology Group, Tucson, Arizona) and Jeremy Rogers (College of Optical Sciences, University of Arizona, Tucson, Arizona) for metrology measurements, and Philip M. Hinz and Johanan L. Codona (Steward Observatory, Tucson, Arizona) for coronagraph discussion. This work was supported by the U.S. Army Research Office.

*Corresponding author.
Electronic address: grovers@optics.arizona.edu

[1] *Optical Vortices*, edited by M. Vasnetsov and K. Staliunas, Horizons in World Physics Vol. 228 (Nova Science, New York, 1999).
[2] A. Ashkin, Biophys. J. **61**, 569 (1992).
[3] V. Westphal and S. W. Hell, Phys. Rev. Lett. **94**, 143903 (2005).
[4] M. Levenson, S. M. Tan, G. Dai, Y. Morikawa, N. Hayashi, and T. Ebihara, in *Proceedings of Optical Microlithography XVI, 2003*, edited by Anthony Yen, Proc. SPIE Int. Soc. Opt. Eng. Vol. 5040 (SPIE-International Society for Optical Engineering, Bellingham, WA, 2003), p. 344.
[5] Y. Liu, D. Liu and J. Hu, in *Proceedings of 24th Annual BACUS Symposium on Photomask Technology, 2004*, edited by Wolfgang Staud, J. Tracy Weed, Proc. SPIE Int. Soc. Opt. Eng. Vol. 5567 (SPIE-International Society for Optical Engineering, Bellingham, WA, 2004), p. 723.
[6] H. H. Arnaut and G. A. Barbosa, Phys. Rev. Lett. **85**, 286 (2000).
[7] A. Mair, A. Vaziri, G. Weihs, and A. Zeilinger, Nature (London) **412**, 313 (2001).
[8] S. Franke-Arnold, S. M. Barnett, M. J. Padgett, and L. Allen, Phys. Rev. A **65**, 033823 (2002).
[9] G. Foo, D. M. Palacios, and G. A. Swartzlander, Opt. Lett. **30**, 3308 (2005).
[10] D. Mawet, P. Riaud, O. Absil, and J. Surdej, Astrophys. J. **633**, 1191 (2005).
[11] M. Pitchumani, H. Hockel, W. Mohammed, and E. G. Johnson, Appl. Opt. **41**, 6176 (2002).
[12] J. W. Sung, H. Hockel, J. D. Brown, and E. G. Johnson, Appl. Opt. **45**, 33 (2006).
[13] G. A. Swartzlander, Jr., Opt. Lett. **31**, 2042 (2006).
[14] Z. Bomzon, G. Biener, V. Kleiner, and E. Hasman, Opt. Lett. **27**, 285 (2002).
[15] D. M. Palacios, in *Proceedings of Techniques and Instrumentation for Detection of Exoplanets II, 2005*, edited by Daniel R. Coulter, Proc. SPIE Int. Soc. Opt. Eng. Vol. 5905 (SPIE-International Society for Optical Engineering, Bellingham, WA, 2005), p. 196.
[16] D. M. Palacios, Opt. Lett. (to be published).
[17] Z. S. Sacks, D. Rozas, and G. A. Swartzlander, Jr., J. Opt. Soc. Am. B **15**, 2226 (1998).
[18] M. V. Berry, J. Opt. A Pure Appl. Opt. **6**, 259 (2004).
[19] G. A. Swartzlander, Jr., Opt. Lett. **30**, 2876 (2005).